Identification of functionally important conserved trans-membrane residues of bacterial P_{IB}-type ATPases.

Daniel Zhitnitsky and Oded Lewinson.

Department of Microbiology,
The Bruce and Ruth Rappaport Faculty of Medicine,
The Technion-Israel Institute of Technology,
Haifa, Israel.

Corresponding author: Oded Lewinson
e-mail: lewinson@tx.technion.ac.il; telephone: +972-4-8295428; fax: +972-4-8295205

Running title: Functionally important residues of P_{IB}-type ATPases.

Keyword: Transport, Permeability, Metal homeostasis, Membrane proteins, Membrane transport, Transition metals, P-type ATPases.

This article has been accepted for publication and undergone full peer review but has not been through the copyediting, typesetting, pagination and proofreading process, which may lead to differences between this version and the Version of Record. Please cite this article as doi: doi/10.1111/mmi.12495

ABSTRACT

Powered by ATP hydrolysis, P_{IB}-ATPases drive the energetically uphill transport of transition metals. These high affinity pumps are essential for heavy metal detoxification and delivery of metal cofactors to specific cellular compartments.

Amino acid sequence alignment of the trans-membrane (TM) helices of P_{IB}-ATPases reveals a high degree of conservation, with ~60-70 fully conserved positions. Of these conserved positions, 6-7 were previously identified to be important for transport. However, the functional importance of the majority of the conserved TM residues remains unclear.

To investigate the role of conserved TM residues of P_{IB}-ATPases we conducted an extensive mutagenesis study of a Zn^{2+}/Cd^{2+} P_{IB}-ATPase from *Rhizobium radiobacter* (rrZntA) and seven other P_{IB}-ATPases. Of the 38 conserved positions tested, 24 had small effects on metal tolerance. 14 mutations compromised *in-vivo* metal tolerance and *in-vitro* metal-stimulated ATPase activity.

Based on structural modeling, the functionally important residues line a constricted 'channel', tightly surrounded by the residues that were found to be inconsequential for function. We tentatively propose that the distribution of the mutable and immutable residues marks a possible trans-membrane metal translocation pathway. In addition, by substituting six trans-membrane amino acids of rrZntA we changed the *in-vivo* metal specificity of this pump from Zn^{2+}/Cd^{2+} to Ag^{+}.

INTRODUCTION

P-type ATPases are a ubiquitous family of trans-membrane ATPases that are found in all extant phyla. Using the energy derived from ATP hydrolysis, these pumps catalyze many transport processes across the various cell membranes. Notable eukaryotic examples include the sarcoplasmic reticulum Ca^{2+} pump, the Na^{+}/K^{+} ATPase, and the gastric proton pump. 'Heavy metal ATPases', or P_{IB}-Type ATPases, transport monovalent and divalent transition metal ions such as Cu^{+}, Ag^{+}, Zn^{2+}, Cd^{2+} and Pb^{2+}. Transition metals such as Cu^{+} and Zn^{2+} are essential co-factors to many cellular functions(1,2), yet they are needed in very small amounts. At high intracellular concentrations all transition metals are highly toxic. In humans, mutations in the Cu^{+}-transporting ATP7A and ATP7B genes can lead to severe pathologies (Menkes and Wilson diseases, respectively). In prokaryotes, P_{IB}-Type ATPases play an important role in metal detoxification. In addition, P_{IB}-Type ATPases contribute to the virulence of many pathogens (3-7) and recent studies suggest that host's macrophages actively increase the concentrations of zinc and copper within the phagosomes (8-11). These new findings may explain why *Mycobacterium tuberculosis* harbors 12 P_{IB}-Type ATPases, as opposed to 5 in the closely related non-pathogenic *Mycobacterium smegmatis (10).*

There are two main substrate-specific subclasses among transition metal P_{IB}-Type ATPases: one subclass (P_{IB1}) transports monovalent metals (Cu^{+} and Ag^{+}) while another (P_{IB2}) transports the divalent metals (Zn^{2+}, Cd^{2+}, Hg^{2+}, and Pb^{2+}).

P_{IB}-Type ATPases are single-chain polypeptides with a distinct structure: An intracellular soluble domain fused to an 8 helices trans-membrane domain (TMD). The intracellular soluble domain includes the catalytic domain responsible for ATP binding and hydrolysis and 1-6 soluble metal-binding domains (MBDs). The TMD harbor a high affinity metal binding site, with an invariably conserved CPC, CPH or SPC metal binding motif in TM6 (12,13). This motif has been shown to be absolutely essential for transports in all P_{IB}-Type ATPases studied to date.

The role of the soluble MBDs is less clear and seem to vary between different systems: In the *E. coli* CopA and ZntA, the MBDs do not seem to have a role in metal selectivity, and are not essential for function (14,15). Conversely, it has been proposed that the soluble MBDs interact with the actuator domain and/or the trans-membrane metal binding site and regulate transport turn over and kinetics (16,17)

In the cyanobacterium *Synechocystis PCC*, the soluble metal binding domains have been shown to affect metal selectivity both directly and indirectly (18,19). Swapping the soluble MBDs of CoaT (Co^{2+} transport) and ZiaA (Zn^{2+} transport) of) resulted in inversion of transport specificity (19) .

In eukaryotes, the soluble MBDs do not seem to have a role in metal selectivity, but rather play a role in copper-regulated trafficking of Cu^+ pumps from intracellular compartments to the plasma membrane (20,21).

Amino acid sequence alignment of trans-membrane (TM) helices 3-8 of P_{IB}-ATPases reveals a high degree of conservation, with ~65 conserved positions in Zn^{2+}/Cd^{2+} pumps, and ~40 in Cu^+/Ag^+ pumps. While some positions are identically conserved irrespective of transport specificity, others are differentially conserved within each substrate-specific subgroup (Figure 1). The CPC motif in TM 6 has long been recognized as essential to the function of both Cu^+/Ag^+ and Zn^{2+}/Cd^{2+} pumps, and is pivotal to metal coordination. In Cu^+/Ag^+ pumps four other conserved TM residues have been identified to be important for transport (Tyr and Asn of TM7, Met and Ser of TM8 (22,23). In pumps of Zn^{2+}/Cd^{2+}, three TM residues have been identified to be important for transport (24-26). However, the majority of conserved TM residues remain uncharacterized and it is thus unclear whether additional positions are essential for transport activity.

To address this question, we have performed an extensive mutational analysis of the Rhizobium radiobacter Zn^{2+}/Cd^{2+} P_{IB}-type ATPase (hereafter rrZntA) and also partially of 7 other prokaryotic Cu^+/Ag^+ and Zn^{2+}/Cd^{2+} P_{IB}-type ATPases. This comparative functional analysis identified 14 conserved amino acids that were important for function. Based on 3-D homology modeling, the distribution of the mutable and immutable residues marks a possible trans-membrane metal translocation pathway. By substituting six conserved amino acids of rrZntA with residues that are conserved in Cu^+/Ag^+ pumps we generated a mutant that conferred cells with robust Ag^+ tolerance.

EXPERIMENTAL PROCEDURES

Amino acid alignment and 3D modeling: Multiple amino acid alignment was done using the ClustalW2 server (European Bioinformatics institute). The 3-D model of rrZntA was generated by the SWISS-MODEL server (Swiss institute of bioinformatics, (27-29)), using the structure of lpCopA as a template.

Cloning and Site direct mutagenesis: The construction of the plasmids encoding the P_{IB} pumps were described elsewhere (30,31). Whole plasmid site direct mutagenesis was performed using a commercial kit (QuikChange™ Lightning, Stratagene) or by using separately obtained PfuUltra™ (Agilent), DpnI (NEB) and dNTPs (Sigma). Primers were synthesized by Syntezza Bioscience, Israel. The correct insertion of all mutations (and lack of additional undesired mutations) was verified by sequencing

Metal sensitivity assays: Metal sensitive *E. coli* strains GG44 (Cu^{+}/Ag^{+} sensitive) and GG48 (Zn^{+2}/Cd^{2+} sensitive) were used (32,33). Cells transformed with the indicated plasmids were grown at 37˚C in LB medium containing Ampicillin (100 µg/ml) and Kanamycin (30 µg/ml). The cells were then diluted to an OD_{600} of 0.05 in 150µl of the same media, containing L-Arabinose (0.02%) and in the presence or absence of metal salts ($CuSO_4$, $ZnSO_4$ or $CdCl_2$). Metal sensitivity with $AgNO_3$ was performed in a similar manner, but in Davis minimal medium. Growth was monitored continuously for 10 hours in an automated plate reader (Infinite M200 pro, Tecan). Growth percentage of each mutant was calculated from growth profile of each variant, using Simpson's rule of integration. The difference in the growth between the wild type variant and the negative control (empty plasmid) was defined as 100% activity, and all mutants are expressed as relative percent.

Metal sensitivity assays on solid media were performed by adding 1.5% Agar to same media as described above. Cells were grown in a similar manner and diluted to an OD600 of 0.1. Three 10-fold dilutions were performed and applied drop-wise (1.5µl) on top of the agar medium.

Estimation of membrane-fraction expression levels: BL21RIPL Cells were grown at 37˚C in 10ml of LB media containing Ampicillin (100 µg/ml) and Kanamycin (30 µg/ml) until an OD600 of ~1. L-Arabinose was then added (0.2%), and the cells were grown for an additional 1 hour. Cells were then harvested and re-suspended in 1ml of 50mM Tris PH 8, 150mM NaCl and 1mM PMSF. Cells were disrupted using a tip sonicator, and un-lysed cells, debris and inclusion bodies were removed by centrifugation at 17,000 g. Membranes were collected by ultracentrifugation at 150,000 g, and re-suspended in 50mM Tris PH 8, 150mM NaCl and 1mM PMSF, 10% glycerol. Expression was then verified by SDS-PAGE and western blot analysis (using anti-His antibodies).

Preparation of inverted vesicles and ATPase assays: BL21RIPL Cells were grown and harvested as described for the expression verification. They were then re-suspended in 1ml of 20mM Tris PH 7.5, 100mM NaCl, 0.03 mg/ml DNAse, 2mM $MgCl_2$ and protein inhibitor cocktail. Inverted vesicles were prepared as described above (expression validation). The membranes were then washed with same buffer, without $MgCl_2$, and after ultracentrifugation re-suspended in same buffer (without $MgCl_2$) containing 10% glycerol. Protein concentration was determined using a nanodrop 2000 (Thermo scientific) and membranes were frozen in liquid nitrogen and stored in -80°C.

The ATPase assay was performed using a commercial EnzChek® Phosphate Assay Kit (Molecular probes), essentially as previously described (34,35). The Reaction buffer contained 0.25 mM 2-amino-6-mercapto-7-methylpurine riboside (MESG), 1 U/ml purine nucleoside phosphorylase (PNP), 2 mM $MgCl_2$, 2.5mM dithiothreitol (DTT), 5 mM Cysteine, 150 µg membrane vesicles and either 0 µM or

150 µM of $Pb(NO_3)_2$. The reaction was incubated at 37˚C in an automated plate reader (Infinite M200 pro, Tecan) for 15 – 30 min, until the signal stabilized, and the assay started by injecting 1 mM ATP. Total metal activation effect was calculated by subtracting the ATP hydrolysis rate obtained in the absence of $Pb(NO_3)_2$ from that obtained in the presence of it.

RESULTS

Amino acid residues chosen for mutational analysis.

As our goal was to identify conserved TM residues that are essential for function we focused on TM helices 3-8 which show a high degree of sequence conservation (Figure 1). A comparison of Cu^+/Ag^+ and Zn^{2+}/Cd^{2+} ATPases reveals a large number of amino acid positions that are similarly conserved in both these two subgroups. Such residues may perhaps be involved in mechanistic features that are unrelated to metal specificity, such as E1-E2 conformational changes. In addition to residues that are similarly conserved in both substrate-specific subgroups, we identified TMD positions where the conservation was specific to each subgroup (i.e, differentially conserved amino acids). An example for such a residue is the conserved TM5 Pro of Zn^{2+}/Cd^{2+} ATPases that is replaced by a Trp in Cu^+/Ag ATPases. We hypothesized that such differentially conserved residues may be involved (directly or indirectly) in metal selectivity. Other conserved TM positions are specifically conserved within a substrate-specific subclass but have no conserved counterparts in the other subclass. An example for such residues is the conserved TM6 triad Trp-Ile-Tyr of Zn^{2+}/Cd^{2+} ATPases. A total of 38 residues were chosen for mutagenesis (Figure 1) representing these three categories of conserved residues. Among the chosen residues we also included several that have been previously shown to be essential for function in homologous systems (to serve as internal controls).

Mutational analysis of rrZntA.

Initially, the 38 chosen residues were mutated to alanine in rrZntA (UniProtKB Q7D0J8). We chose to begin with rrZntA since a metal-sensitive *E. coli* strain expressing rrZntA from a plasmid has a very robust growth phenotype with both Zn^{2+} and Cd^{2+} (30). The activity of the mutants was characterized using metal-tolerance growth assays in liquid media. These assays require relatively little manual handling and can be performed in a semi high throughput manner using an automated plate reader. In addition, the *in-vivo* beneficial effect of rrZntA is hardly affected by its expression level, and maximal metal tolerance is achieved even at low expression (Figure 2A&B). This is important as we expected a certain degree of variability in the expression level of the different mutants.

We tested the membrane-fraction expression of all mutants (see methods), and observed that all mutants expressed at levels comparable to that of wild type rrZntA, with largely similar band patterns (Supplementary Figure 1). These two observations indicate that the observed *in-vivo* differences between the metal-tolerance levels conveyed by each mutant can be used as a proxy for their relative activity.

In the presence of toxic concentrations of Zn^{2+} or Cd^{2+}, the large growth advantage of cells expressing wild-type rrZntA readily allowed the identification of mutants with full, partial, or no activity (Figure 3A). At first, all mutants were tested for Zn^{2+}-tolerance in a broad range of concentrations. In each experiment we calculated the area bound between the growth curves of wild type rrZntA and the vector control. This area was defined as 100% activity. We next calculated the area bound between the growth curves of the each of the mutants and that of the vector control, and these were expressed as per-cent relative to the area defined as 100%. Mutants displaying a growth area of at least 75% (relative to wild type) were categorized as having normal growth, and were not studied further. Those displaying growth less than 75% (relative to wild type) were additionally tested in a range of Cd^{2+} concentrations. Mutants displaying at least a two-fold reduction of growth (i.e., 50% of wild type) in the presence of at least one metal (Zn^{2+}or Cd^{2+}) were considered as having compromised metal tolerance. Figure 3B&C show a few examples of such growth experiments while Table 1 summarizes the complete mutational analysis.

Of the 38 tested positions, 24 mutants displayed a growth phenotype that was ≥75% of wild-type rrZntA, and were consequently categorized as residues that do not have a major role in transport (Table 1, and small black arrows in Figure 1). 14 mutants showed at least a two-fold reduction in metal tolerance (with at least one metal), and were hence categorized as harboring mutations in functionally important residues (bold text in Table 1, small red arrows in Figure 1). Among these 14 (as expected), were 5 previously described residues: the canonical Cys-Pro-Cys (TM6), Lys861 (TM7), and Asp882 (TM8).

The 9 other mutations that reduced metal tolerance (to varying extents) are Glu366Ala, Val370Ala, Glu381Ala, Tyr518Ala, Arg547Ala, Ile562Ala, Ser563Ala, Leu860Ala, and Thr868Ala.

Of these, the mutations in Glu381 and Glu366 had the greatest effect on metal tolerance.

To verify that the observed effects of the mutations were not specific to growth in liquid media we also performed metal tolerance experiments in solid media. As shown (Figure 4), largely comparable results were obtained.

Spatial positioning of residues important for function.

To assess the spatial positioning of the residues found to be important for metal tolerance a 3-D model of rrZntA was constructed based on the X-ray structure of lpCopA (36). lpCopA was crystallized in its E2-Pi conformation, and this is of course reflected in the model (see also discussion regarding the model, its reliability and interpretation).

According to this homology model, a possible trans-membrane permeation pathway is formed by TM helices 4, 6, 7, and 8. Conspicuously, all of the 14 residues that were identified as being important for function line this possible pathway (Figure 5A). The 24 residues found to be inconsequential for metal tolerance are located more toward the exterior of the protein, surrounding this putative permeation pathway (Figure 5B).

Relative to the membrane plane, the two glutamates are positioned above and below the CPC metal binding motif. Glu381 is located at the cytosolic side of the TM4, while Glu361 is located toward the periplasmic end of the same helix. Ile562 and Ser563 are invariably conserved in Zn^{2+}/Cd^{2+} ATPases, and are located at TM6 3aa from the CPC metal binding motif, towards the cytosol. The same positions are also invariably conserved in Cu^{+}/Ag^{+} ATPases, but here the conservation is to Leu and Ala, respectively (Figure 1). Tyr518 is located at the same height of the CPC motif and its hydroxyl points directly towards it.

Lys861 (invariably conserved in Zn^{2+}/Cd^{2+} ATPases) is located in TM7, ~ 4 Å away from the CPC motif. The same position is invariably an Asn in Cu^{+}/Ag^{+} ATPases, and this Asn has been demonstrated to be important for ion translocation (22,23).

Arg547 is found on the extracellular side of TM6 near Thr868 of TM7. The positive charge of this arginine is conserved only in Zn^{2+}/Cd^{2+} ATPases. The 14 residues found to be important for metal tolerance are spread along an axis that is roughly perpendicular to the membrane plane, and cover the approximate span of the membrane (Figure 5A).

Functional conservation of the identified residues.

Originally, our goal was to identify TM residues whose functional importance is conserved. We thus tested the functional importance of the residues identified in rrZntA also in homologous Cd^{2+}/Zn^{2+} pumps: CzcP, CadA, and ZntA from *Ralstonia metallidurans* (33,37), and ZntA of *E. coli* (38).

In rmZntA mutations in either of the two glutamates led to a pronounced decrease in metal tolerance (Table II). Similar results were also observed with rmCadA, where the effects were even more dramatic. In addition, mutants of rmCadA in I641, S642, and K943 also displayed a much-

reduced metal tolerance profile (Table II, supplementary Figures 2). Compromised metal tolerance (yet to a lesser degree) was also observed in rmCzcP upon mutations in the two glutamates and in I641. In ecZntA the most dramatic effect on metal tolerance was of the K963A mutation (K861 in rrZntA). Mutations in E202, E217, I398, and S399 also led to a decrease in metal tolerance, but these effects were milder and were more pronounced with Cd^{2+} (Table II, Supplementary Figure 2).

The two glutamates that were identified as important for metal tolerance of Zn^{2+}/Cd^{2+} pumps are of special interest. First, their location relative to the central CPC metal-binding motif makes them potential suspect of coordinating ion entry and exit to and from the main site. In addition, both glutamates are invariably conserved also in Cu^{+}/Ag^{+} ATPases.

To investigate the role of the two glutamates in Cu^{+}/Ag^{+} ATPases, mutants were generated in three such pumps: *Rhizobium radiobacter* CopA and CopB and *Pyrococcus furiosus* CopA (30). In all three proteins, Cu^{+}-tolerance was not greatly affected by mutations in either of the glutamates (Table II). In contrast, Ag^{+}-tolerance was reduced by the mutations (Figure 6, Table II). The most pronounced effects were of the E270A mutation in pfCopA and of E297A of rrCopB. In these two cases the growth of the mutant was very similar to the growth of cells transformed with an empty (control) plasmid (Figure 6, Table II). A complete failure to grow was observed with an rrZntA mutant where both glutamates were mutated to alanines. The growth of this mutant was indistinguishable from that of the negative control, with both Zn^{2+} and Cd^{2+} (Table I).

We also investigated (in rrZntA) the effect of conservative replacements of the two glutamates (Glu>Asp or Glu>Gln). Relative to the non-conservative Glu/Ala substitution, retention of a charged or hydrophilic side chain led to a more wild type like resistance profile. With both Zn^{2+} and Cd^{2+}, mutants E366D, E366Q, E381D, and E381Q, performed significantly better than their alanine-substituted counterparts (Table I, supplementary Figure 3).

***ATP hydrolysis by wild type and mutant rrZntA*.**

P-type ATPases are characterized by low uncoupled ATPase activity that is stimulated in the presence of substrate. In mutants with impaired metal recognition (or impaired E1/E2 transitions) this substrate-induced stimulation is not observed (12,25,38). To investigate metal-stimulated ATPase activity we have taken advantage of the high expression levels of rrZntA in *E. coli* membranes (31). We prepared inverted membrane vesicles from *E. coli* cells transformed with a plasmid encoding wild type rrZntA (pBAD-rrZntA), and measured their ATP hydrolytic activity in the absence or presence of Pb^{2+} We chose Pb^{2+} since it was previously demonstrated that this transition metal has the greatest effect in stimulating the basal ATPase activity of Zn^{2+}/Cd^{+2} P_{IB}-type ATPases (26,38). Supplementary Figure 4

shows the ATPase activity in the absence or presence of Pb^{2+} of wild type rrZntA, the negative control, and mutants, while Figure 7 shows the net difference (presence minus absence of Pb^{2+}). As shown, a clear difference was observed with wild type rrZntA. To verify that indeed this difference is related to the activity of rrZntA we also prepared membrane vesicles from cells transformed with a control (empty) plasmid and from cells transformed with plasmid pBAD-rrZntA but where protein expression was not induced (no addition of L-arabinose during growth). In both these preparations, we did not detect a stimulation of ATP hydrolysis in the presence of Pb^{2+} (Figure 7A, Supplementary Figure 3). Immunoblot analysis of the membranes used in these ATPase assays revealed that the Pb^{2+}-stimulated ATPase activity corresponds to the presence/absence of rrZntA in the membrane (inset in Figure 7A). To further test the specificity of the above assay we tested the Pb^{2+}-stimulated ATPase activity of a mutant rrZntA where the essential Asp of the P-type signature DKTG motif (D600) was replaced with alanine. In addition we also tested the effect of a mutation in the conserved CPC motif (C555A). As shown in Figure 7B, both these mutants had very low Pb^{2+}-stimulated ATPase activity. Taken together, we conclude that the observed Pb^{2+}-stimulated ATPase activity is indeed related to the activity of functional rrZntA.

We next prepared membrane vesicles from cells over-expressing the rrZntA mutants that were identified to be important for metal-tolerance. As an additional control we also tested the Pb^{2+}-stimulated ATPase activity of a mutant with unaltered metal tolerance (Leu550Ala). Initial rates (first 90 seconds) of ATP hydrolysis in the absence or presence of Pb^{2+} were measured for all variants.

Figure 7B and supplementary Figures 4&5 show that the Pb^{2+}-stimulated ATPase activity of wild-type rrZntA and the mutants roughly segregates into three levels of activities: The highest level of Pb^{2+}-stimulated ATPase was observed with wild type rrZntA and with the L550A mutant (the mutation that did not affect metal tolerance). Four mutants (I562A, S563A, R547A, and T868A) show an intermediate level of activity, partially retaining their response to metal. The Pb^{2+}-stimulated ATPase activity of E366A, V370, E381A, L860A, K861A, and D882A was very low and segregated with that of C555A (CPC motif mutant) and D600A (DKTG motif mutant). Overall, the magnitude of the effect of the mutations on the Pb^{2+}-stimulated ATPase activity correlated reasonably well with their effect on *in-vivo* metal resistance.

***Generation of an rrZntA mutant with specificity to silver*.**

rrZntA shares ~36% overall amino acid sequence identity with pumps of Cu^{+}/Ag^{+}, yet the conservation is mostly limited to the soluble catalytic N, A, and P domains. The sequence identity of the TMs is much lower (~10%). We nevertheless attempted to identify a minimal set of trans-membrane amino

acid substitutions that will change the selectivity of rrZntA from Zn^{2+}/Cd^{2+} to Cu^{+}/Ag^{+}. We first introduced four residues that have been reported to be important for monovalent metal recognition: the Tyr and Asn of TM7, and the Met and Ser of TM8 (22,23). However, the resulting mutant (L860Y/K861N/V889M/A893S) had no appreciable activity with either Cu^{+} or Ag^{+} as judged by metal tolerance experiments (Supplementary Table I). We made an additional substitution that introduced a Met residue in TM3. Based on the structure of lpCopA, this Met residue was proposed to be part of the ion entry site (36). Nevertheless, this variant (I347M/L860Y/K861N/V889M/A893S) also did not have any appreciable activity. We then took out this Met substitution and instead substituted the essential Asp882 (TM8) of rrZntA with a Pro residue. Although this proline has no known function, it is invariably conserved in pumps of Cu^{+}/Ag^{+} (Figure 1). Similar to what we observed with the previous constructs, we did not detect any appreciable activity with this one (L860Y/K861N/D882P/V889M/A893S) either. In a final attempt, we combined the two latter substitutions and generated a construct with a total of six substitutions: I347M /L860Y/K861N/D882P/V889M/A893S. Of the six mutations present in this mutant three are in residues that we found to be important for Zn^{2+}/Cd^{2+} tolerance and metal-stimulated ATPase activity (L860, K861, D882, Table I). Not surprisingly, this mutant lost all ability to confer Zn^{2+}/Cd^{2+} tolerance (not shown). On the other hand, the mutant conferred robust Ag^{+} tolerance: in the presence of 4.5 μM $AgNO_3$ the growth of this mutant was 7-fold greater than that of wild-type rrZntA, and ~30-fold greater than that of cells transformed with a control plasmid (Figure 8). Surprisingly, the altered metal specificity did not extend to Cu^{+}, towards which no tolerance was observed (Supplementary Table I).

DISCUSSION

The trans-membrane helices of P_{IB}-ATPases contain a large number of conserved amino acids. Our goal in this work was to identify which of these are essential for function.

We reasoned that an alanine substitution of an essential residue will lead to reduced *in-vivo* metal tolerance, while that of a non-essential one will not.

We generated a total of 58 alanine substitutions (representing 38 conserved positions) in 8 P_{IB}-ATPses (Tables I&II) in positions predicted to be in the core TMs (TMs 3-8). This mutational screen identified 14 conserved TM residues that were important for metal tolerance (9 novel, 5 previously described). Perhaps in testimony of the robustness of the *in-vivo* assay, all of the previously described residues implicated in transport activity were among these 14. Of the residues that had the greatest effect on activity of pumps of Zn^{2+}/Cd^{2+} five are also shared by pumps of Ag^{+}/Cu^{+} (CPC and the two

glutamates). Moreover, of the ~240 TM residues of rrZntA six substitutions were sufficient to shift the specificity of this Zn^{2+}/Cd^{2+} pump towards Ag^{+}. These two observations imply mechanistic conservation and suggest similarities in metal coordination. The main metal-coordinating residues are probably similar between P_{IB1} and P_{IB2} ATPases yet the fine-tuning of selectivity is provided by auxiliary residues. In this regard, it is noteworthy that in generating the Ag^{+}-tolerant rrZntA mutant we had to remove the "hard" Lewis base/acid of Lys861 and D882. Both had to be replaced with "softer" Lewis ligands.

With respect to previously identified conserved TM residues, our results agree with reports describing the importance of Lys of TM7 and Asp of TM8 of Zn^{2+}/Cd^{2+} pumps (26). As shown here mutating this TM7 Lys had a truly dramatic effect on metal tolerance and metal-stimulated ATPase in all tested homologues. Although lysine is not a common ligand of Zn^{2+}/Cd^{2+}, a direct role for metal recognition cannot be excluded. A MESPEUS search (39) yields 87 examples of Zn^{2+} coordination by lysine. An Asn substitution of this lysine in *E. coli* ZntA yielded a mutant that had no measurable ATPase activity, a greatly reduced Zn-dependent phosphorylation by ATP, and hyper-phosphorylation by Pi that was largely insensitive to Zn (24). However, since metal binding stabilizes the E1 conformation these results can also be interpreted by a preference of this mutant toward the E2 conformation over E1. Irrespective of the interpretation, it is clear that the conserved Lys of TM7 plays a direct and important role in metal translocation. Interestingly, in the lipid P-type ATPase ATP8A2 the Lys in this position has been shown to be essential for lipid transport. In ATP8A2 (40), mutant K873A displayed much reduced ATPase and transport activities, but was phosphorylated at a rate similar to wild type. Further, the authors also demonstrated that the mutant has reduced affinity to phosphatidylserine. Taken together, these results suggest a direct role for K873 in lipid recognition.

The location of the Lys of TM7 is very similar to that of the site I metal-coordinating residues of the Ca^{2+}-ATPase and Na^{+}/K^{+}-ATPase (41-45). In the Na^{+}/K^{+}-ATPase a similarly located serine directly participates in K^{+} binding, while in the Ca^{2+}-ATPase an asparagine serves as a ligand for Ca^{2+}. In the H^{+}/K^{+}-ATPase the homologous lysine residue (K800) is crucial for proper H^{+}/K^{+} transport stoichiometry and is thus also implicated in metal recognition (46). Thus, while the exact mechanistic details may vary, the conservation of this TM7 position underscores a degree of mechanistic uniformity between Type-I, Type-II, and Type-IV P-type-ATPases.

Among the nine residues were newly identified as being important for function are three non-plolar residues (Val370, Ile562, and Leu860) and three polar residues (Tyr518, Ser563, and Thr868). Relative to the effects of mutations in the charged residues (E366, E381, D882, K861) mutations in

these residues resulted in milder effects (Table I). This may indicate a supportive, rather than a main role in metal translocation. Carbonyl oxygens of Val, Leu and Ile have been demonstrated in the past to participate in coordination of Zn^{2+} (47-50). Relative to the membrane plane, the carbonyl oxygen of Ile562, the carboxyl of Glu381, and the hydroxyl of Ser563 are at the same height. Possibly, these form together an electronegative field for the initial attraction of the metal. The carbonyl oxygen of Val370 is within close proximity of C558 of the CPC, plausibly contributing an additional ligand to the central metal coordination site. The Carbonyl oxygen of Leu860 is too far to participate in any of the clusters of potential metal ligands, and it is unlikely involved in metal coordination. We suspect that Leu860 may have a role in the proper orientation of the adjacent Lys861, which is pivotal for function. Thr868 is located on the same helix as Lys861, but towards the periplasm. The hydroxyl group of threonine often serves as a Zn^{2+} ligand. It is also conspicuously positioned right across and 4.2Å away from the carbonyl oxygen of Arg547 (also a characterized Zn^{2+} ligand). Possibly, the hydroxyl of Thr868 and the carbonyl oxygen of Arg547 provide an electrostatic pull, swaying and guiding the metal from the CPC motif to the exit. The amino side chain of Arg547 points away from the plane of interaction between Thr868 and the carbonyl oxygen of Arg547. The location of this positive charge may serve to block an alternative exit pathway between helices 5, 6, and 7.

The carboxylate oxygen of glutamic acid is a very common Zn^{2+} ligand, and the strong phenotype we report here of mutants of the two TM 4 glutamates suggests a central role for these two residues. Based on the structure of lpCopA, Gourdon *et al* suggested that these glutamates (Glu189 and Glu205 in lpCopA) are part the trans-membrane metal entry (Glu205) and exit (Glu189) sites (36). The location of Glu366 & Glu381 in the 3-D model of rrZntA supports this suggestion. Possibly, Glu381 participates in initial metal recognition/attraction in the E1 conformation, while E366 participates in metal release from the CPC metal binding site during the transition to E2P.

More recently, it was also demonstrated that Glu205 of the *Archaeoglobus fulgidus* Cu^{+}-ATPase (afCopA) participates in initial metal recognition and relay of metal from the copper chaperone afCopZ to the central CPC metal binding motif (51).

Although it is not common, Glu residues have been demonstrated to participate in coordination of Cu^{+} (52-55). In the three tested Cu^{+}/Ag^{+} pumps, mutation in one or two of the glutamate led to an interesting phenotype, affecting Ag^{+} tolerance by a much larger degree than Cu^{+} tolerance (Table II). We do not know the reason for this difference. Both metals have very similar Pauling electronegativity values (1.9 for Cu, 1.93 for Ag). Although it is possible that this small difference is responsible for the observed phenotypes, we find it unlikely.

Without exception, all of the mutants that displayed attenuated metal tolerance also displayed reduced Pb^{2+}-stimulated ATPase activity, and we observed good agreement in the degree a given mutation affected these two phenotypes.

Compromised *in-vivo* metal tolerance can stem from several factors, such as reduced expression/stability of the mutant, defective E1-E2 conformational changes, and defective metal recognition. The activity/expression results presented in Figure 2 strongly argue against the former. However, the growth assays and the metal-stimulated ATPase experiments cannot differentiate between mutants with defective E1-E2 transitions or with impaired metal recognition. Despite the possible roles (detailed above) in metal coordination of the non-polar (and perhaps polar) residues, it is entirely plausible that several of these have functions that are unrelated to metal coordination.

To visualize the spatial distribution of the mutable vs. the immutable residues we constructed a 3-D model of rrZntA based on the X-ray structure of lpCopA. Several factors limit the reliability of such modeling. First, lpCopA is a Cu^{+}/Ag^{+} pump while rrZntA transports Zn^{2+}/Cd^{2+}. Second, the structure of lpCopA was determined in its E2-Pi conformation, and the TM helices will occupy different positions in the E1 state. This is especially pertinent when considering metal binding since it occurs when the protein is in E1. Nevertheless, despite these limitations, we do not believe that the spatial distribution of the functionally important residues (vs. the unimportant ones) displayed in the 3-D model is coincidental and/or insignificant. 'Business-end' residues are expected to be close to, or line the metal permeation pathway while less important residues are more likely to be found in the periphery. In the 3-D model, a trans-membrane permeation pathway is formed by helices 4, 6, 7, and 8. Without exception, all of the 14 residues that were identified as being important for function line this possible pathway.

ACKNOWLEDGMENTS

We thank Chris Rensing for his kind gift of *E. coli* metal sensitive strains, Dietrich H. Nies for his gift of the plasmids encoding the *Ralstonia metallidurans* P-type ATPases, and Gabriele Meloni for stimulating discussions.

This work was supported in part by grants from the Israeli Academy of Sciences, and the Rappaport Family Institute for Biomedical Research.

The authors declare no conflict of interest.

REFERENCES

1. Andreini, C., Bertini, I., Cavallaro, G., Holliday, G., and Thornton, J. (2008) Metal ions in biological catalysis: from enzyme databases to general principles. Journal of Biological Inorganic Chemistry 13, 1205-1218

2. Festa, R. A., and Thiele, D. J. (2011) Copper: an essential metal in biology. Curr Biol 21, R877-883

3. Klein, J. S., and Lewinson, O. (2011) Bacterial ATP-driven transporters of transition metals: physiological roles, mechanisms of action, and roles in bacterial virulence. Metallomics 3, 1098-1108

4. Francis, M. S., and Thomas, C. J. (1997) Mutants in the CtpA copper transporting P-type ATPase reduce virulence of Listeria monocytogenes. Microb Pathog 22, 67-78

5. González-Guerrero, M., Raimunda, D., Cheng, X., and Argüello, J. M. (2010) Distinct functional roles of homologous Cu+ efflux ATPases in Pseudomonas aeruginosa. Mol Microbiol 78, 1246-1258

6. Ward, S. K., Abomoelak, B., Hoye, E. A., Steinberg, H., and Talaat, A. M. (2010) CtpV: a putative copper exporter required for full virulence of Mycobacterium tuberculosis. Mol Microbiol 77, 1096-1110

7. McLaughlin, H. P., Xiao, Q., Rea, R. B., Pi, H., Casey, P. G., Darby, T., Charbit, A., Sleator, R. D., Joyce, S. A., Cowart, R. E., Hill, C., Klebba, P. E., and Gahan, C. G. (2012) A putative P-type ATPase required for virulence and resistance to haem toxicity in Listeria monocytogenes. PLoS One 7, e30928

8. White, C., Lee, J., Kambe, T., Fritsche, K., and Petris, M. J. (2009) A role for the ATP7A copper-transporting ATPase in macrophage bactericidal activity. J Biol Chem 284, 33949-33956

9. Botella, H., Peyron, P., Levillain, F., Poincloux, R., Poquet, Y., Brandli, I., Wang, C., Tailleux, L., Tilleul, S., Charrière, G. M., Waddell, S. J., Foti, M., Lugo-Villarino, G., Gao, Q., Maridonneau-Parini, I., Butcher, P. D., Castagnoli, P. R., Gicquel, B., de Chastellier, C., and Neyrolles, O. (2011) Mycobacterial p(1)-type ATPases mediate resistance to zinc poisoning in human macrophages. Cell Host Microbe 10, 248-259

10. Botella, H., Stadthagen, G., Lugo-Villarino, G., de Chastellier, C., and Neyrolles, O. (2012) Metallobiology of host-pathogen interactions: an intoxicating new insight. Trends Microbiol 20, 106-112

11. Festa, R. A., and Thiele, D. J. (2012) Copper at the front line of the host-pathogen battle. PLoS Pathog 8, e1002887

12. Dutta, S. J., Liu, J., Stemmler, A. J., and Mitra, B. (2007) Conservative and nonconservative mutations of the transmembrane CPC motif in ZntA: effect on metal selectivity and activity. Biochemistry 46, 3692-3703

13. Argüello, J. M., Eren, E., and González-Guerrero, M. (2007) The structure and function of heavy metal transport P1B-ATPases. Biometals 20, 233-248

14. Fan, B., and Rosen, B. P. (2002) Biochemical Characterization of CopA, the Escherichia coli Cu(I)-translocating P-type ATPase. Journal of Biological Chemistry 277, 46987-46992

15. Mitra, B., and Sharma, R. (2001) The cysteine-rich amino-terminal domain of ZntA, a Pb(II)/Zn(II)/Cd(II)-translocating ATPase from Escherichia coli, is not essential for its function. Biochemistry 40, 7694-7699

16. Tsivkovskii, R., MacArthur, B. C., and Lutsenko, S. (2001) The Lys1010–Lys1325 Fragment of the Wilson's Disease Protein Binds Nucleotides and Interacts with the N-terminal Domain of This Protein in a Copper-dependent Manner. Journal of Biological Chemistry 276, 2234-2242

17. Mandal, A. K., and Argüello, J. M. (2003) Functional Roles of Metal Binding Domains of the Archaeoglobus fulgidus Cu+-ATPase CopA†. Biochemistry 42, 11040-11047

18. Tottey, S., Patterson, C. J., Banci, L., Bertini, I., Felli, I. C., Pavelkova, A., Dainty, S. J., Pernil, R., Waldron, K. J., Foster, A. W., and Robinson, N. J. (2012) Cyanobacterial metallochaperone inhibits deleterious side reactions of copper. Proceedings of the National Academy of Sciences 109, 95-100

19. Borrelly, G. P. M., Rondet, S. A. M., Tottey, S., and Robinson, N. J. (2004) Chimeras of P1-type ATPases and their transcriptional regulators: contributions of a cytosolic amino-terminal domain to metal specificity. Molecular Microbiology 53, 217-227

20. Forbes, J. R., Hsi, G., and Cox, D. W. (1999) Role of the Copper-binding Domain in the Copper Transport Function of ATP7B, the P-type ATPase Defective in Wilson Disease. Journal of Biological Chemistry 274, 12408-12413

21. Forbes, J. R., and Cox, D. W. (2000) Copper-dependent trafficking of Wilson disease mutant ATP7B proteins. Human Molecular Genetics 9, 1927-1935

22. González-Guerrero, M., Eren, E., Rawat, S., Stemmler, T. L., and Argüello, J. M. (2008) Structure of the two transmembrane Cu+ transport sites of the Cu+ -ATPases. J Biol Chem 283, 29753-29759

23. Mandal, A. K., Yang, Y., Kertesz, T. M., and Argüello, J. M. (2004) Identification of the transmembrane metal binding site in Cu+-transporting PIB-type ATPases. J Biol Chem 279, 54802-54807

24. Liu, J., Dutta, S. J., Stemmler, A. J., and Mitra, B. (2006) Metal-binding affinity of the transmembrane site in ZntA: implications for metal selectivity. Biochemistry 45, 763-772

25. Dutta, S. J., Liu, J., Hou, Z., and Mitra, B. (2006) Conserved aspartic acid 714 in transmembrane segment 8 of the ZntA subgroup of P1B-type ATPases is a metal-binding residue. Biochemistry 45, 5923-5931

26. Okkeri, J., and Haltia, T. (2006) The metal-binding sites of the zinc-transporting P-type ATPase of Escherichia coli. Lys693 and Asp714 in the seventh and eighth transmembrane segments of ZntA contribute to the coupling of metal binding and ATPase activity. Biochim Biophys Acta 1757, 1485-1495

27. Arnold, K., Bordoli, L., Kopp, J., and Schwede, T. (2006) The SWISS-MODEL workspace: a web-based environment for protein structure homology modelling. Bioinformatics 22, 195-201

28. Bordoli, L., Kiefer, F., Arnold, K., Benkert, P., Battey, J., and Schwede, T. (2009) Protein structure homology modeling using SWISS-MODEL workspace. Nat Protoc 4, 1-13

29. Bordoli, L., and Schwede, T. (2012) Automated protein structure modeling with SWISS-MODEL Workspace and the Protein Model Portal. Methods Mol Biol 857, 107-136

30. Lewinson, O., Lee, A. T., and Rees, D. C. (2009) A P-type ATPase importer that discriminates between essential and toxic transition metals. Proceedings of the National Academy of Sciences 106, 4677-4682

31. Lewinson, O., Lee, A. T., and Rees, D. C. (2008) The funnel approach to the precrystallization production of membrane proteins. J Mol Biol 377, 62-73

32. Grass, G., Fan, B., Rosen, B. P., Franke, S., Nies, D. H., and Rensing, C. (2001) ZitB (YbgR), a member of the cation diffusion facilitator family, is an additional zinc transporter in Escherichia coli. J Bacteriol 183, 4664-4667

33. Scherer, J., and Nies, D. H. (2009) CzcP is a novel efflux system contributing to transition metal resistance in Cupriavidus metallidurans CH34. Mol Microbiol 73, 601-621

34. Tal, N., Ovcharenko, E., and Lewinson, O. (2013) A single intact ATPase site of the ABC transporter BtuCD drives 5% transport activity yet supports full in vivo vitamin B12 utilization. Proceedings of the National Academy of Sciences 110, 5434-5439

35. Vigonsky, E., Ovcharenko, E., and Lewinson, O. (2013) Two molybdate/tungstate ABC transporters that interact very differently with their substrate binding proteins. Proceedings of the National Academy of Sciences 110, 5440-5445

36. Gourdon, P., Liu, X. Y., Skjørringe, T., Morth, J. P., Møller, L. B., Pedersen, B. P., and Nissen, P. (2011) Crystal structure of a copper-transporting PIB-type ATPase. Nature 475, 59-64

37. Legatzki, A., Grass, G., Anton, A., Rensing, C., and Nies, D. H. (2003) Interplay of the Czc system and two P-type ATPases in conferring metal resistance to Ralstonia metallidurans. J Bacteriol 185, 4354-4361

38. Sharma, R., Rensing, C., Rosen, B. P., and Mitra, B. (2000) The ATP hydrolytic activity of purified ZntA, a Pb(II)/Cd(II)/Zn(II)-translocating ATPase from Escherichia coli. J Biol Chem 275, 3873-3878

39. Harding, M., and Hsin, K.-Y. (2014) Mespeus—A Database of Metal Interactions with Proteins. in Structural Genomics (Chen, Y. W. ed.), Humana Press. pp 333-342

40. Coleman, J. A., Vestergaard, A. L., Molday, R. S., Vilsen, B., and Andersen, J. P. (2012) Critical role of a transmembrane lysine in aminophospholipid transport by mammalian photoreceptor P4-ATPase ATP8A2. Proc Natl Acad Sci U S A 109, 1449-1454

41. Toyoshima, C. (2009) How Ca2+-ATPase pumps ions across the sarcoplasmic reticulum membrane. Biochimica et Biophysica Acta (BBA) - Molecular Cell Research 1793, 941-946

42. Toyoshima, C., Kanai, R., and Cornelius, F. (2011) First Crystal Structures of Na+,K+-ATPase: New Light on the Oldest Ion Pump. Structure 19, 1732-1738

43. Møller, J. V., Nissen, P., Sørensen, T. L. M., and Maire, M. l. (2005) Transport mechanism of the sarcoplasmic reticulum Ca2+-ATPase pump. Current Opinion in Structural Biology 15, 387-393

44. Schack, V. R., Morth, J. P., Toustrup-Jensen, M. S., Anthonisen, A. N., Nissen, P., Andersen, J. P., and Vilsen, B. (2008) Identification and Function of a Cytoplasmic K+ Site of the Na+, K+-ATPase. Journal of Biological Chemistry 283, 27982-27990

45. Morth, J. P., Pedersen, B. P., Toustrup-Jensen, M. S., Sorensen, T. L.-M., Petersen, J., Andersen, J. P., Vilsen, B., and Nissen, P. (2007) Crystal structure of the sodium-potassium pump. Nature 450, 1043-1049

46. Burnay, M., Crambert, G., Kharoubi-Hess, S., Geering, K., and Horisberger, J.-D. (2003) Electrogenicity of Na,K- and H,K-ATPase Activity and Presence of a Positively Charged Amino Acid in the Fifth Transmembrane Segment. Journal of Biological Chemistry 278, 19237-19244

47. Linden, A., Mayans, O., Meyer-Klaucke, W., Antranikian, G., and Wilmanns, M. (2003) Differential Regulation of a Hyperthermophilic α-Amylase with a Novel (Ca,Zn) Two-metal Center by Zinc. Journal of Biological Chemistry 278, 9875-9884

48. Reverter, D., Fernandez-Catalan, C., Baumgartner, R., Pfander, R., Huber, R., Bode, W., Vendrell, J., Holak, T. A., and Aviles, F. X. (2000
) Structure of a novel leech carboxypeptidase inhibitor determined free in solution and in complex with human carboxypeptidase A2. Nat Struct Mol Biol 7, 322-328
49. Suzuki, H., Kawasaki, M., Inuzuka, T., Okumura, M., Kakiuchi, T., Shibata, H., Wakatsuki, S., and Maki, M. (2008) Structural Basis for Ca2+-Dependent Formation of ALG-2/Alix Peptide Complex: Ca2+/EF3-Driven Arginine Switch Mechanism. Structure 16, 1562-1573
50. Wintjens, R., Belrhali, H., Clantin, B., Azarkan, M., Bompard, C., Baeyens-Volant, D., Looze, Y., and Villeret, V. (2006) Crystal Structure of Papaya Glutaminyl Cyclase, an Archetype for Plant and Bacterial Glutaminyl Cyclases. Journal of Molecular Biology 357, 457-470
51. Padilla-Benavides, T., McCann, C. J., and Argüello, J. M. (2013) The mechanism of Cu+ transport ATPases: interaction with CU+ chaperones and the role of transient metal-binding sites. J Biol Chem 288, 69-78
52. Lieberman, R. L., Arciero, D. M., Hooper, A. B., and Rosenzweig, A. C. (2001) Crystal Structure of a Novel Red Copper Protein from Nitrosomonas europaea†,‡. Biochemistry 40, 5674-5681
53. Qin, L., Liu, J., Mills, D. A., Proshlyakov, D. A., Hiser, C., and Ferguson-Miller, S. (2009) Redox-Dependent Conformational Changes in Cytochrome c Oxidase Suggest a Gating Mechanism for Proton Uptake. Biochemistry 48, 5121-5130
54. Koepke, J., Olkhova, E., Angerer, H., Müller, H., Peng, G., and Michel, H. (2009) High resolution crystal structure of Paracoccus denitrificans cytochrome c oxidase: New insights into the active site and the proton transfer pathways. Biochimica et Biophysica Acta (BBA) - Bioenergetics 1787, 635-645
55. Steiner, R. A., Kooter, I. M., and Dijkstra, B. W. (2002) Functional Analysis of the Copper-Dependent Quercetin 2,3-Dioxygenase. 1. Ligand-Induced Coordination Changes Probed by X-ray Crystallography: Inhibition, Ordering Effect, and Mechanistic Insights†. Biochemistry 41, 7955-7962

FIGURE AND TABLE LEGENDS.

Table 1. Relative growth of rrZntA mutants. Except where indicated, the values shown are for the alanine substitution. Growth was calculated as percent relative to the growth of wild type rrZntA (see text and methods for details). In bold are residues found to be important for *in-vivo* metal tolerance. Errors are standard deviations, n=3.
nd: not determined.

Table 2. Relative growth of mutant variants of Cu^+/Ag^+ and Zn^{2+}/Cd^{2+} pumps. Growth was calculated as percent relative to the growth of the wild type of each of the homologues (see text and methods for details). na: not applicable.

Figure 1. Amino acid sequence alignment of TMs 3-8 of 14 PIB-type ATPases (7 Cu^+/Ag^+ pumps, 4 Zn^{2+}/Cd^{2+} pumps, and 3 Cd^{2+} pumps). Amino acids that are conserved throughout are highlighted in yellow. Amino acids conserved only in pumps of Cu^+/Ag^+ are highlighted in magenta, while those specific to Zn^{2+}/Cd^{2+} or Cd^{2+} pumps are highlighted in cyan. Small arrows indicate positions that were chosen for mutagenesis (red arrows: residues later found to be important for function, black arrows: those found to be unimportant for function).

Figure 2. (A) Growth in liquid media of wild type rrZntA in the absence or presence of L-arabinose. For all cultures, 100% growth was defined as the growth in the absence of metal. Empty vector blue squares, all other symbols are wild type rrZntA grown in the presence of 0% (red squares), 0.0125% (green triangles), 0.025% (black crosses), and 0.05% (cyan circles) L-arabinose (W/V). (B) Western blot detection of the expression of rrZntA in the membrane fraction of *E. coli* cells induced with 0%, 0.001%, 0.005%, 0.01%, and 0.05% L-arabinose (W/V) as indicated.

Figure 3. Growth in liquid media of wild type and mutant rrZntA in the absence or presence of $ZnSO_4$ or $CdCl_2$. In all panels: wild type open squares, I562A closed squares, E366A closed triangles, E381A crosses, K861A open triangles, empty vector circles. (A) Time dependent growth in the presence of 0.3 mM $ZnSO_4$. (B) Relative growth in the presence of the indicated concentrations of $ZnSO_4$. For each culture, 100% was defined as the growth in the absence of metal. (C) Same as B only in the presence of $CdCl_2$. In B&C error bars (shown unless smaller than icons) represent standard deviations of three repeats.

Figure 4. Growth in solid media of wild type and mutant rrZntA. Four 10-fold dilutions were spotted from left to right, in the absence or presence of the indicated concentrations of $ZnSO_4$ or $CdCl_2$.

Figure 5. A 3-D homology model of rrZntA based on the X-ray structure of lpCopA. The TM, N, P, and A domains are colored green, orange, magenta, and yellow, respectively. Amino acids positions that were tested in the mutational screen are shown as spheres: in red are the ones that were found to be important for activity and in blue the ones that weren't. (A) Side view, the functionally important residues are indicated except for Lys 861 and Tyr 518 that are hidden in this view behind Asp 882 and Pro 557. The approximate boundaries of the membrane are indicated by solid black lines. (B) Top view.

Figure 6. Growth in liquid media of wild type and mutant variants of the Cu^+/Ag^+ pumps pfCopA (A), rrCopA (B), rrCopB (C) in the presence of the indicated $AgNO_3$ concentrations. In A, wild type pfCopA open squares, E254A closed triangles, E270A crosses, empty vector closed circles. In B, wild type rrCopA open squares, E274A closed triangles, E290A crosses, empty vector closed circles. In C, wild type rrCopB open squares, E281A closed triangles, E297A crosses, empty vector closed circles. For each culture, 100% was defined as the growth in the absence of metal. In A-C error bars (shown unless smaller than icons) represent standard deviations of three repeats.

Figure 7. Pb^{2+}- stimulated ATP hydrolysis by wild type and mutant rrZntA. (A) Membrane vesicles were prepared from cells transformed with a control plasmid (circles), or from cell transformed with plasmid encoding rrZntA (open or closed squares). Expression of rrZntA was induced (closed squares) or not (open squares) by addition of 0.2% (V/V) L-arabinose. ATP hydrolysis was measured in the presence or absence of 250μM $Pb(NO_3)_2$, and the data shown is the net difference per mg of total membrane protein. 1 mM ATP was injected (at 1 min) to initiate hydrolysis. The inset shows a western blot detection of the same vesicles used in the ATPase assays using an α-His antibody. (B). Initial rates of Pb^{2+}- stimulated ATPase activity of membrane vesicles prepared from cells overexpressing wild type rrZntA (closed squares), and mutants L550A (open squares), I562A (open diamonds), S563A (closed diamonds), E366A (open triangles), E381A (closed circles), C555A (open circles), D600A (closed triangles). The data shown is the net difference (presence vs. absence of 250μM $Pb(NO_3)_2$) per mg of total membrane protein.

Figure 8. An rrZntA mutant that confers Ag^+ tolerance. Cells were transformed with an empty plasmid (circles), plasmid encoding wild type rrZntA (open squares), or plasmid encoding the rrZntA mutant I347M /L860Y/K861N/D882P/V889M/A893S (crosses). Cultures were grown in the absence or presence of the indicated $AgNO_3$ concentrations. Error bars (shown unless smaller than icons) represent standard deviations of six repeats. Also shown are p values derived by a student T. Test.

Table 1

Residue	Zn tolerance	Cd tolerance		Residue	Zn tolerance	Cd tolerance
Arg333	75-100%	75-100%		**Ile562**	49±0.55%	48±0.21%
Ile347	75-100%	nd		**Ser563**	68±4.74%	54±1.5%
Gly362	75-100%	nd		Gln852	75-100%	nd
Glu366	16±0.73%	31±0.16%		Asn853	75-100%	nd
Val370	41±0.54%	38±0.53%		**Leu860**	53±0.23	48±0.34%
Phe374	75-100%	n.d		**Lys861**	11±0.37%	12±0.22%
Glu381	7±0.13%	6±0.04%		**Thr868**	59±5.5%	47±6.8%
Gln512	75-100%	nd		**Asp882**	2%±0.45%	0%
Phe514	75-100%	nd		Thr883	75-100%	nd
Arg516	75-100%	nd		Thr886	75-100%	nd
Tyr518	57±0.43%	47±1.34%		Leu888	75-100%	nd
Pro533	75-100%	nd		Val889	75-100%	nd
Trp544	75-100%	nd		Thr890	75-100%	nd
Ile545	75-100%	nd		Asn892	75-100%	nd
Tyr546	75-100%	nd		Arg895	75-100%	nd
Arg547	73±0.19%	49±0.53%		Leu896	75-100%	nd
Leu551	75-100%	n.d		Glu366/Asp	75-100%	58±0.61%
Cys556	0%	0%		Glu381/Asp	75-100%	75-100%
Pro557	50%	15%		Glu366/Gln	75-100%	75-100%
Cys558	0%	0%		Glu381/Gln	47±3.96%	75-100%
Val561	75-100%	75-100%		Glu366/Ala Glu381/Ala	0±0.086%	0±0.028%

Table 2

	Residue	Zn tolerance	Cd tolerance
R. metallidurans ZntA (Q1LEH0)	E247A	21±0.6%	37±1.24%
	E262A	14±0.13%	0±0.27%
R. metallidurans CadA (Q58AL5)	E444A	0±0.04%	26±0.15%
	E459A	0±0.82%	6±0.25%
	I641A	20±0.43%	5±0.01%
	S642A	23±0.84%	30±0.65%
	K943A	0±0.28%	18±0.07%
R. metallidurans CzcP (Q1LAJ7)	E269A	68±0.72%	na
	E284A	28±0.74%	na
	I641A	45±1.49%	na
E.coli ZntA (P37617)	E202A	73±2.67%	55±0.94%
	E217A	63±4.64%	42±6.45%
	I398A	74±1.07%	44±1.26%
	S399A	82±2.07%	55±1.25%
	K963A	5±0.12%	2±0.08%
	Residue	**Cu tolerance**	**Ag tolerance**
P. fulgidus CopA (O29777)	E254A	82±0.93%	70±0.32%
	E270A	89±2.03%	0±0.53%
R. radiobacter CopA (A9CJE3)	E274A	95±0.72%	29±0.55%
	E290A	98±0.23%	67±3.29%
R. radiobacter CopB (A9CJP7)	E281A	81±0.87%	37±2.53%
	E297A	100±0.68%	14±1.09%

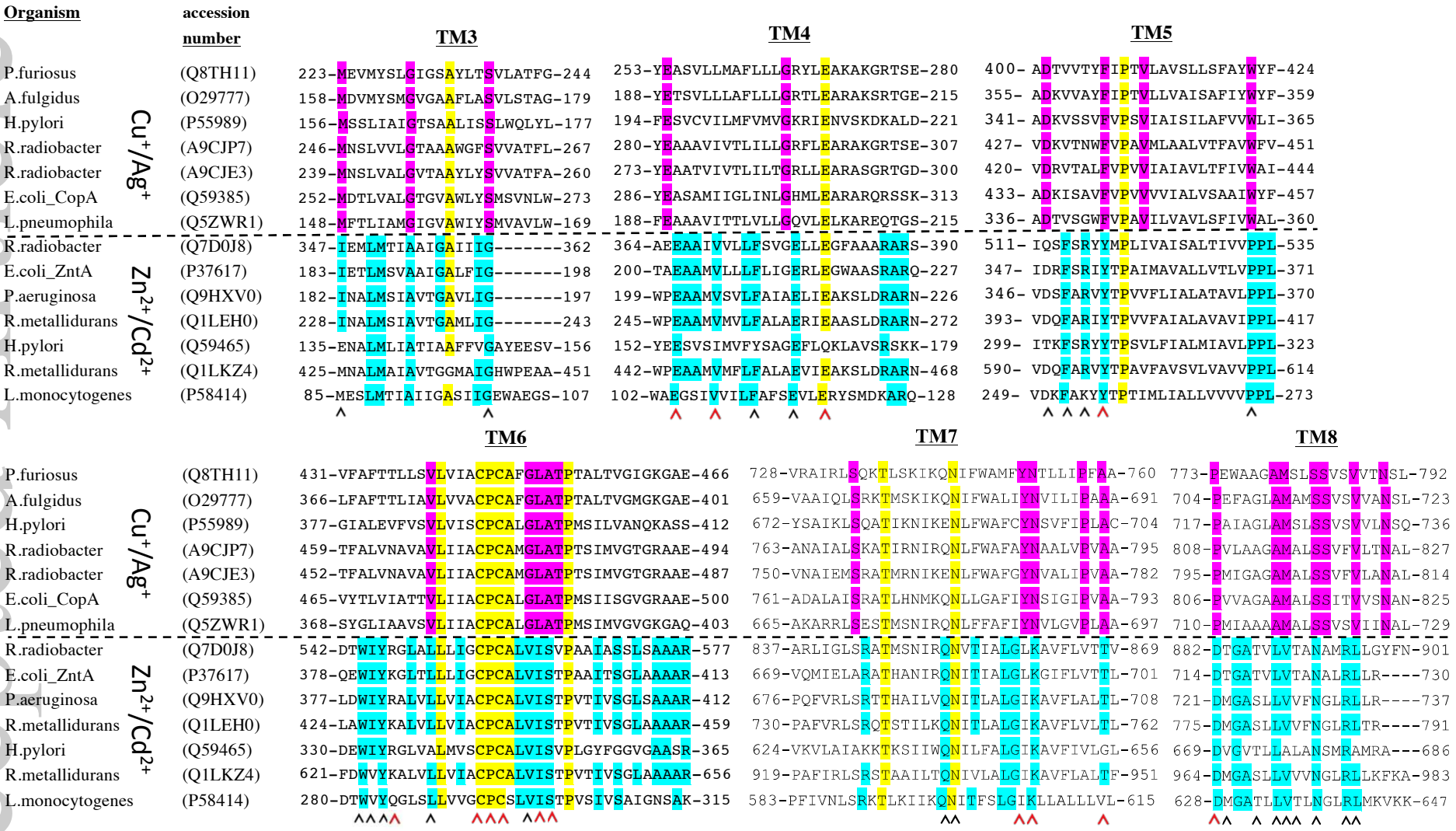

Figure 1

A

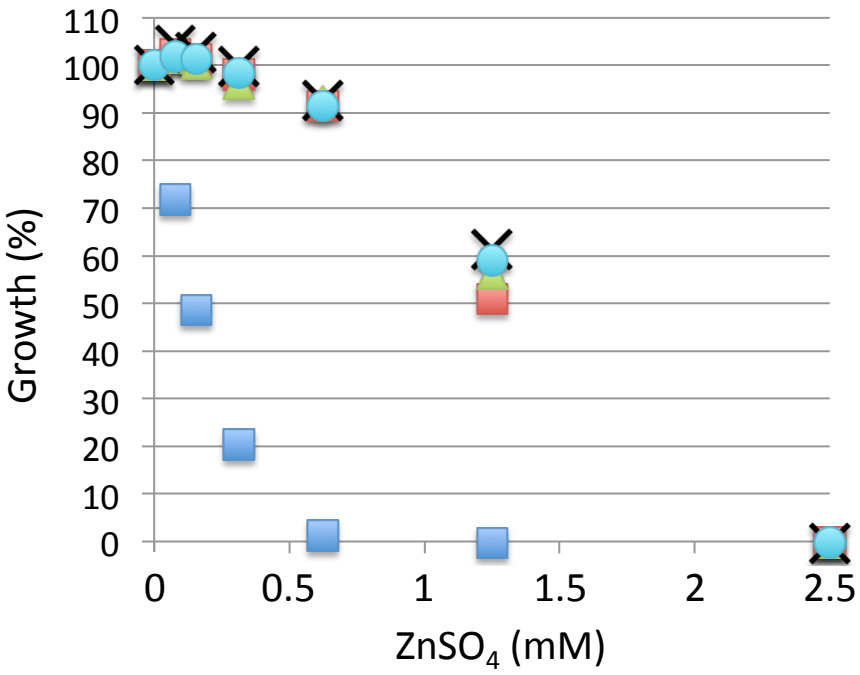
110
100
90
80
70
60
50
40
30
20
10
0
Growth (%)
0
0.5
1
1.5
2
2.5
ZnSO4 (mM)

B

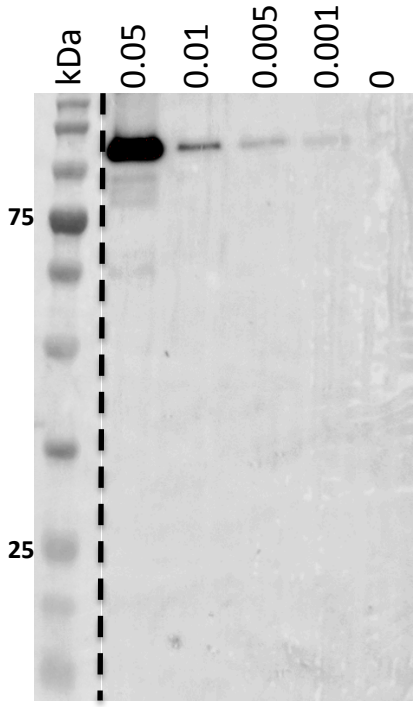
kDa
0.05
0.01
0.005
0.001
0
75
25

Figure 2

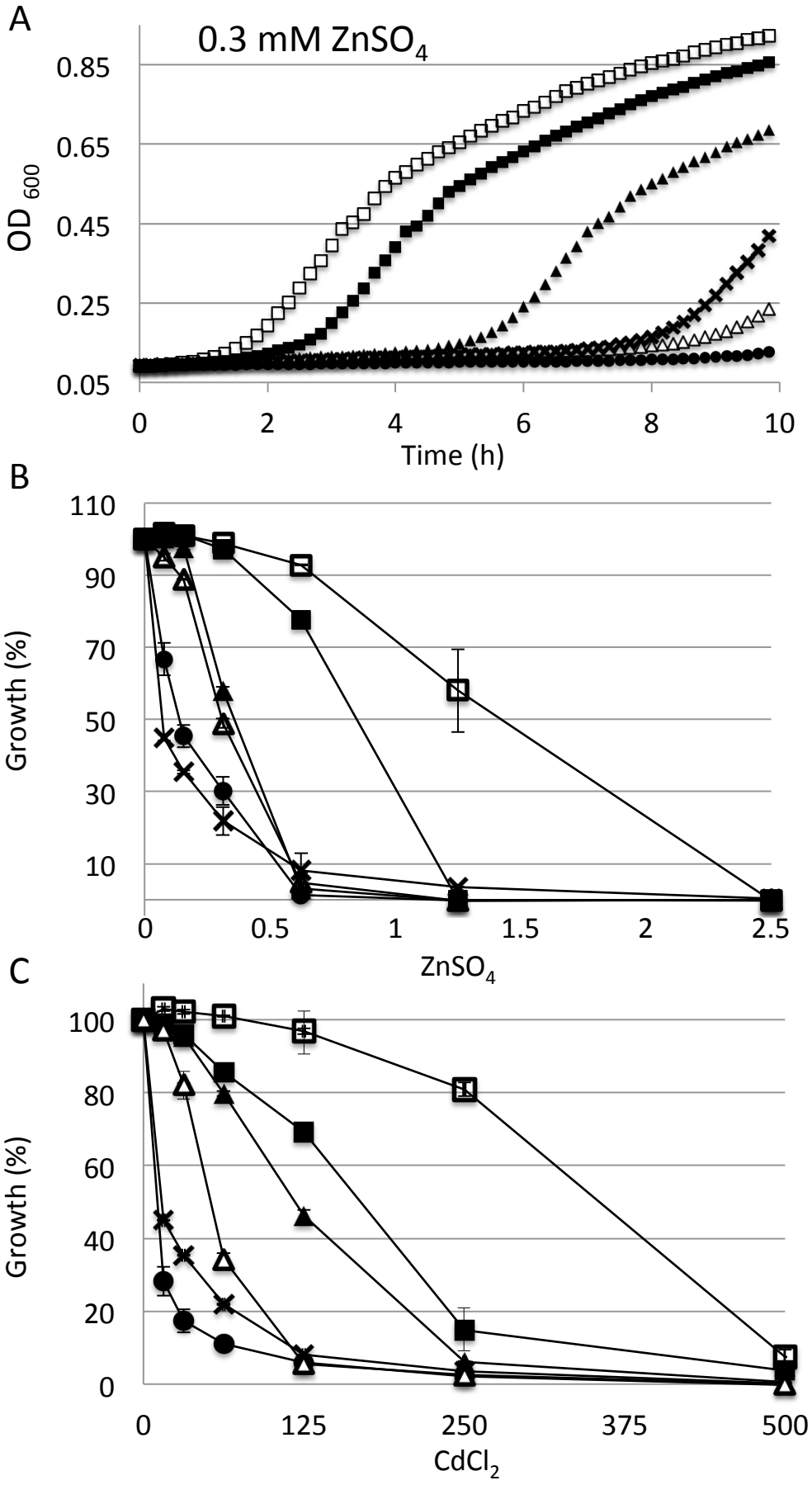
A
0.3 mM ZnSO4
OD 600
0.85
0.65
0.45
0.25
0.05
0
2
4
6
8
10
Time (h)
B
Growth (%)
110
90
70
50
30
10
0
0.5
1
1.5
2
2.5
ZnSO4
C
Growth (%)
100
80
60
40
20
0
0
125
250
375
500
CdCl2

Figure 3

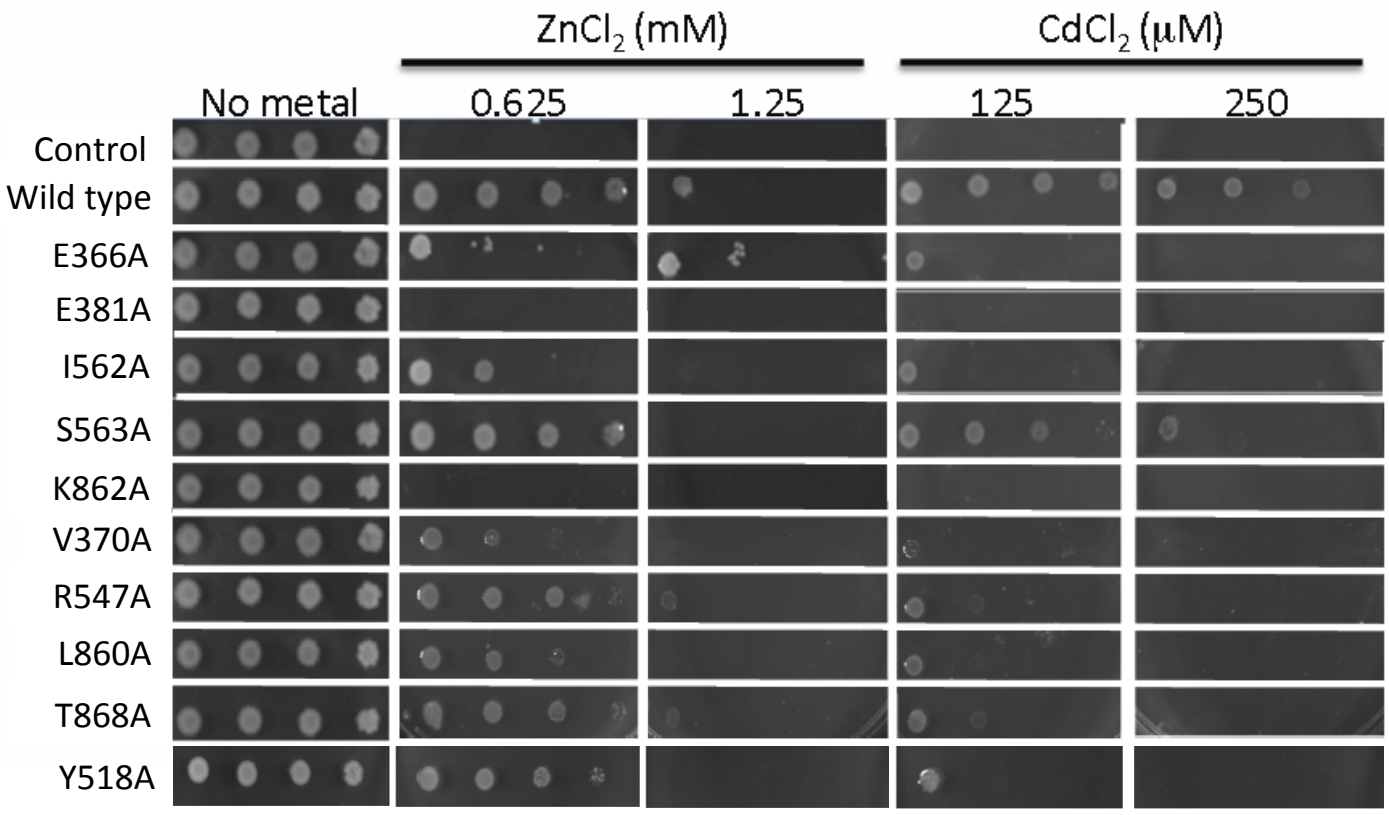
ZnCl2 (mM)
CdCl2 (μM)
No metal
0.625
1.25
125
250
Control
Wild type
E366A
E381A
I562A
S563A
K862A
V370A
R547A
L860A
T868A
Y518A

Figure 4

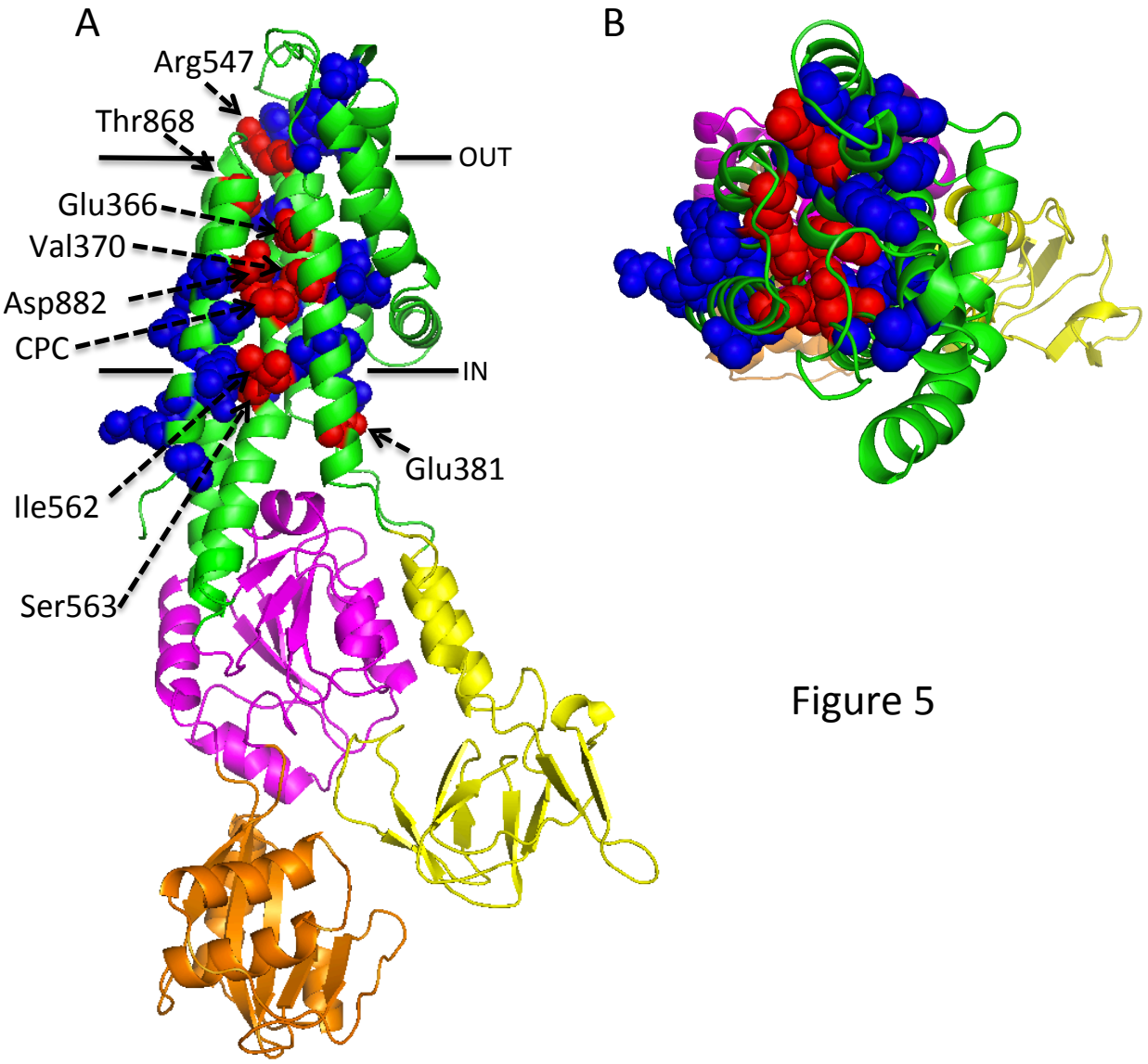
A
Arg547
Thr868
OUT
Glu366
Val370
Asp882
CPC
IN
Glu381
Ile562
Ser563
B

Figure 5

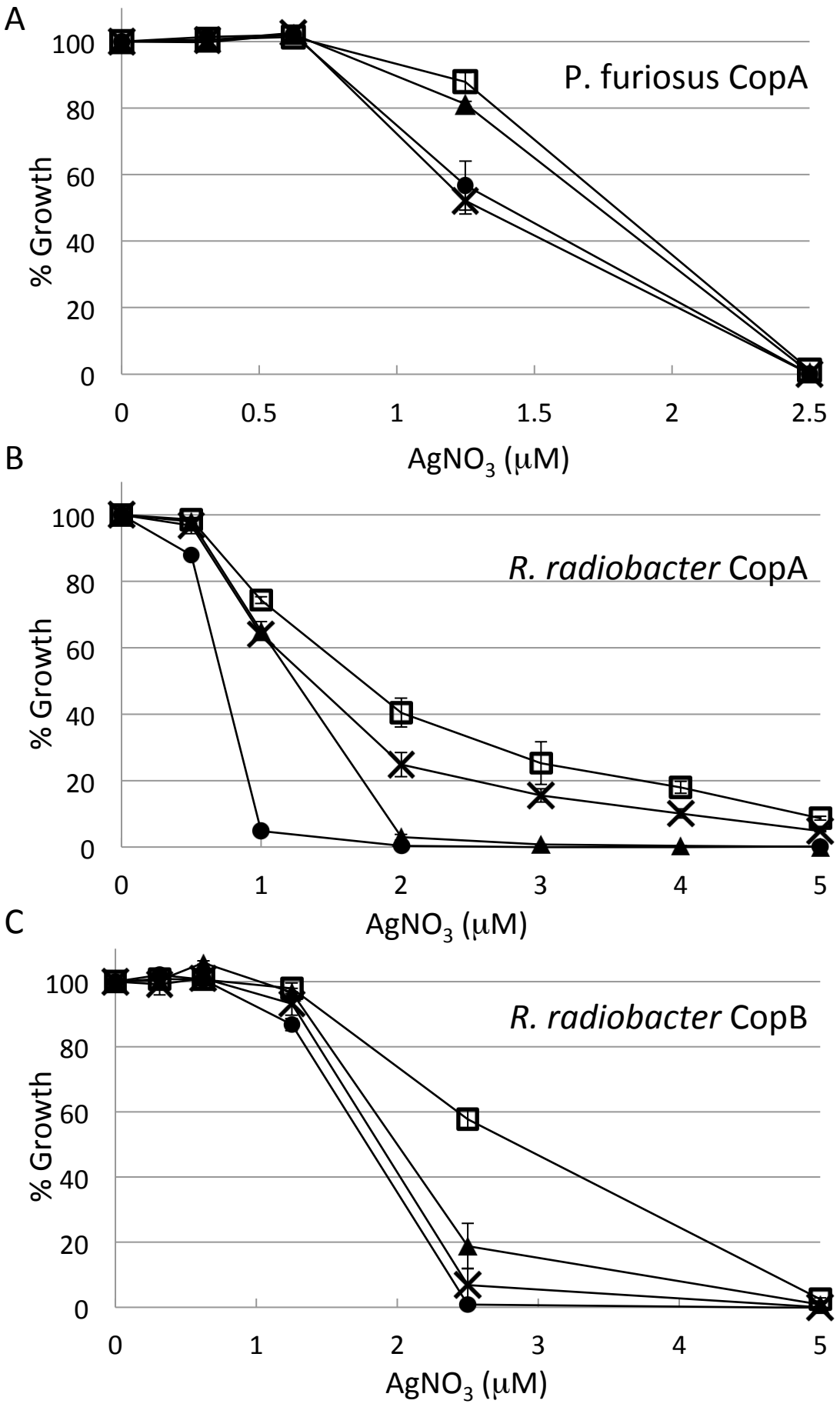
A
P. furiosus CopA
% Growth
100
80
60
40
20
0
0
0.5
1
1.5
2
2.5
AgNO3 (μM)
B
R. radiobacter CopA
% Growth
100
80
60
40
20
0
0
1
2
3
4
5
AgNO3 (μM)
C
R. radiobacter CopB
% Growth
100
80
60
40
20
0
0
1
2
3
4
5
AgNO3 (μM)

Figure 6

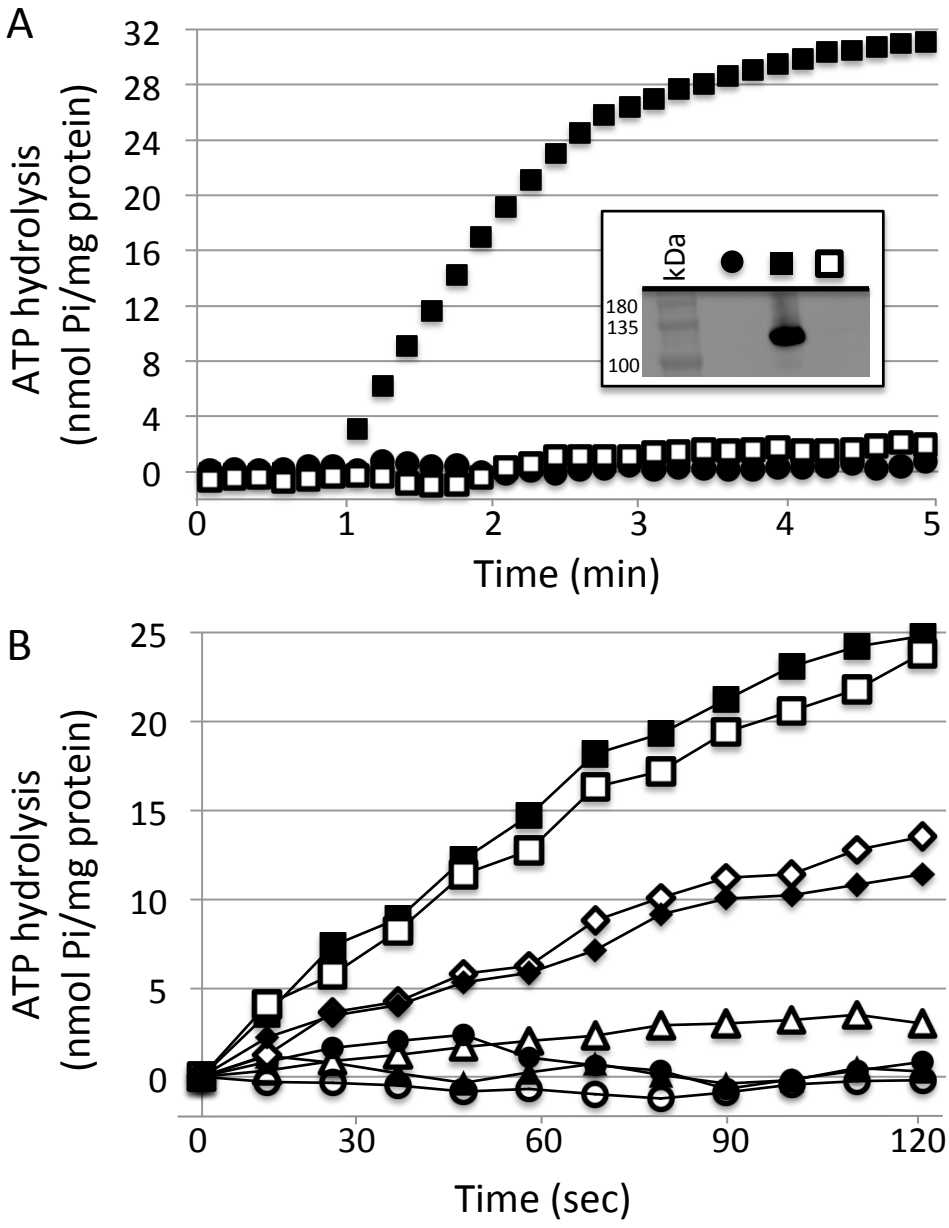
A
ATP hydrolysis (nmol Pi/mg protein)
32
28
24
20
16
12
8
4
0
0
1
2
3
4
5
Time (min)
kDa
180
135
100
B
ATP hydrolysis (nmol Pi/mg protein)
25
20
15
10
5
0
0
30
60
90
120
Time (sec)

Figure 7

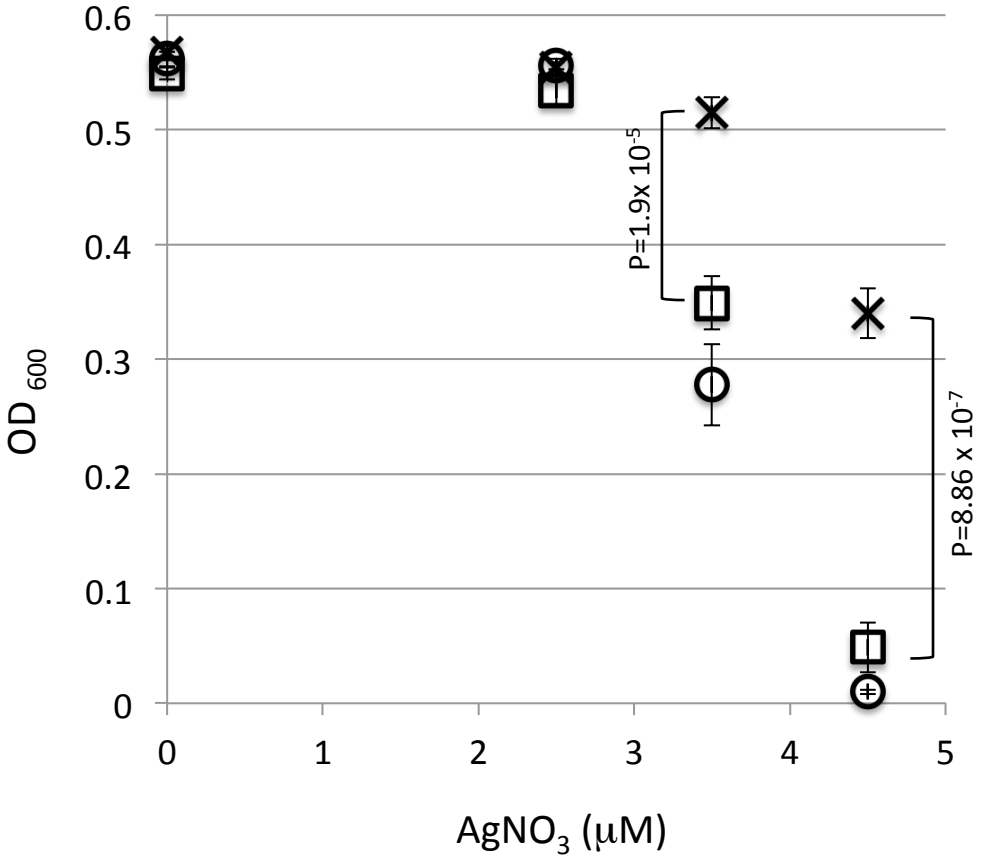

Figure 8